# UC Irvine
## UC Irvine Previously Published Works

**Title**

Yttrium-90 Radioembolization and Tumor Hypoxia: Gas-challenge BOLD Imaging in the VX2 Rabbit Model of Hepatocellular Carcinoma.

**Permalink**

https://escholarship.org/uc/item/8vh0691z

**Journal**

Academic radiology, 28(6)

**ISSN**

1076-6332

**Authors**

Gordon, Andrew C
White, Sarah B
Gates, Vanessa L
et al.

**Publication Date**

2021-06-01

**DOI**

10.1016/j.acra.2020.04.012

Peer reviewed

# Yttrium-90 Radioembolization and Tumor Hypoxia: Gas-challenge BOLD Imaging in the VX2 Rabbit Model of Hepatocellular Carcinoma

**Andrew C. Gordon**[1,2], **Sarah B. White**[3], **Vanessa L. Gates**[1], **Daniel Procissi**[1], **Kathleen R. Harris**[1], **Yihe Yang**[1], **Zhuoli Zhang**[1], **Weiguo Li**[1], **Tianchu Lyu**[1], **Xiaoke Huang**[1], **Reed A. Omary**[5], **Riad Salem**[1,6,7], **Robert J. Lewandowski**[1], **Andrew C. Larson**[1,2]

[1.]Department of Radiology, Northwestern University Feinberg School of Medicine, Chicago, IL, USA

[2.]Department of Biomedical Engineering, Northwestern University, Evanston, IL, USA

[3.]Department of Radiology, Division of Vascular & Interventional Radiology, Medical College of Wisconsin, Milwaukee, WI, USA

[5.]Department of Radiology and Radiological Sciences, Vanderbilt University, Nashville, TN, USA

[6.]Department of Medicine-Hematology/Oncology, Northwestern University Feinberg School of Medicine, Chicago, IL, USA

[7.]Department of Surgery-Organ Transplantation, Northwestern University Feinberg School of Medicine, Chicago, IL, USA

## Abstract

**PURPOSE:** To use a rapid gas-challenge blood oxygen-level dependent (BOLD) MRI exam to evaluate changes in tumor hypoxia after $^{90}$Y radioembolization (Y90) in the VX2 rabbit model.

**MATERIALS and METHODS:** White New Zealand rabbits (n=11) provided a Y90 group (n=6 rabbits) and untreated control group (n=5 rabbits). R2* maps were generated with gas-challenges (O2 / Room Air) at baseline, 1 week, and 2 weeks post-Y90. Laboratory toxicity was evaluated at baseline, 24hrs, 72hrs, 1 week, and 2 weeks. Histology was used to evaluate tumor necrosis on H&E and immunofluorescence imaging was used to assess microvessel density (CD31) and proliferative index (Ki67).

**First Author/Corresponding: Andrew C. Gordon, MD, PhD, address below,** andrew-gordon@northwestern.edu.
**Senior Author: Andrew C. Larson, PhD,** Professor, Department of Radiology, Northwestern University Feinberg School of Medicine, 737 N. Michigan Ave, 16$^{th}$ Floor, Chicago, IL 60611, Tel./fax: (312) 926-3499 / (312) 926-5991, larsonand@gmail.com

**RESULTS:** At baseline, median tumor volumes and time to imaging were similar between groups (p=1.000 and p=0.4512, respectively). The median administered dose was 50.4Gy (95% confidence interval:44.8–55.9). At week 2, mean tumor volumes were 5769.81 versus 643.69 mm$^3$ for control versus Y90 rabbits, respectively (p=0.0246). At two weeks, R2* increased for control tumors to $12.37\pm12.36\text{sec}^{-1}$ and decreased to $4.48\pm9.00\text{sec}^{-1}$ after Y90. The Pearson correlation coefficient for R2* at baseline and percent increase in tumor size by two weeks was 0.798 for the Y90 group (p=0.002). There was no difference in mean microvessel density for control versus Y90 treated tumors (p=0.6682). The mean proliferative index was reduced in Y90 treated tumors at 30.5% versus 47.5% for controls (p=0.0071).

**CONCLUSION:** The baseline R2* of tumors prior to Y90 may be a predictive imaging biomarker of tumor response and treatment of these tumors with Y90 may influence tumor oxygenation over time.

### Keywords

oxygenation; hepatic radioembolization; magnetic resonance imaging; yttrium-90

## INTRODUCTION

Radioembolization with glass or resin yttrium-90 microspheres (Y90) infused through the hepatic artery delivers selective internal radiation therapy to tumors supplied by these vessels. Re-oxygenation of tumors is a tenet of fractionated radiotherapy because radiation induced damage to tumors is mediated by oxygenation; however, the oxygenation status of tumors prior to radioembolization is not typically assessed nor optimized prior to treatment. Central necrosis due to chronic diffusion-limited hypoxia, excepting primary intrahepatic cholangiocarcinoma (1–3), is a prevalent finding in both primary and metastatic hepatic tumors (4–6). This is especially true for HCC, where necrosis is a common finding in the variant subtypes (7) and is present in up to 97% of patients with large tumors (8). Use of a hypoxia scoring system based on genetic analyses of tumor hypoxia gene signatures has been proposed and appears to retrospectively stratify prognosis in HCC patients (9) but this strategy has not been evaluated prospectively nor become part of clinical paradigm. Furthermore, non-invasive methods for measuring liver tumor hypoxia are not yet established clinically nor validated at the preclinical level.

The purpose of this pilot study was to use a rapid gas-challenge blood oxygen-level dependent (BOLD) MRI exam to evaluate changes in tumor hypoxia after Y90 in the VX2 rabbit model. We hypothesized that increased hypoxia at baseline may limit antitumor activity of therapy and that radiation-induced changes may influence the hypoxic status of VX2 tumors over time.

## MATERIALS AND METHODS

### Study Design

Our institution's animal care and use committee approved this study, and all procedures were performed under institutional and ARRIVE guidelines. The use of glass $^{90}$Y microspheres for research was approved and overseen by the Radiation Safety Officers of

the university and associated hospital system. A total of 9 female and 2 male White New Zealand rabbits weighing 3 to 3.5 kg were scanned for this study (Covance Laboratories, Greenfield, IN). Rabbits underwent VX2 implantation and tumors were allowed to grow to 1–2 cm; each animal was scanned with magnetic resonance imaging (MRI) to confirm tumor growth prior to treatment. The Y90 group was imaged weekly for 2 weeks and the control group was imaged at baseline and at 2 weeks. Tissue specimens, including liver and tumor, were harvested for histopathology and immunofluorescence imaging.

### VX2 Animal Model and US-guided Tumor Implantation

The implemented approach for ultrasound-guided tumor fragment implantation has been previously described in detail (10). There were a total of 3 hepatic implantation sites per rabbit.

### MR Imaging Protocols

Tumor growth was confirmed on MRI. All MRI studies were performed at 7 Tesla using a 20-cm bore Bruker ClinScan magnet (Bruker Biospin MRI GmbH, Ettlingen, Germany) with sequences listed in Table 1. Respiratory gated, free-breathing acquisitions in both the coronal and axial planes were performed.

For gas-challenge imaging with whole tumor coverage during BOLD GRE scans, rabbits were given 98% O2 at 1L/min and 2% isoflurane via nose cone for oxygen scans for 15 minutes followed by room air (78% N2, 20% O2) at 1L/min and 2% isoflurane for 10 minutes prior to and during room air (RA) scans. Susceptibility mapping for R2* (1/T2*) was performed within each voxel according to the Levenberg-Marquardt algorithm to fit the mono-exponential signal decay $S(TE)=M_o exp(–TE \cdot R2^*)$. The change in R2* with gas-challenge was calculated by subtracting the mean R2* during oxygen breathing (R2*$_{O2}$) from the mean R2* during room air breathing (R2*$_{RA}$):

$$\Delta R2^* = R2^*_{RA} - R2^*_{O2}.$$

Regions of interest (ROI) were drawn on the first echo image for R2*$_{RA}$ and R2*$_{O2}$ images and the mean value within these volumes was calculated for each tumor at baseline, 1 week, and 2 weeks.   R2* served as an imaging surrogate for hypoxia (11). Previous work has also associated changes in gas-challenge BOLD signal with fibrosis (12). It is possible that fibrosis may ultimately alter hepatic blood volumes so we evaluated the degree of fibrosis within the treated normal liver on pathology by Masson's trichrome stain.

### Blood Draws

Whole blood was obtained from the ear vein at baseline (MRI scan), 24hrs, 72hrs, 7-days (1-week MRI), and 14-days (2-week MRI) post-treatment. The serum panel included albumin, alkaline phosphatase, alanine aminotransferase (ALT), aspartate aminotransferase (AST), creatine kinase (CK), and total bilirubin.

### Intra-arterial Therapy and [90]Y Radioembolization Dosimetry

Microcatheter systems and wires allowed selective catheterization of hepatic arterial vasculature. Following radioembolization, the delivered dose was calculated as previously described (13). For additional details, please see our Supplemental Methods Section.

### Necropsy & Histopathology

After completion MRI at the 2-week study endpoint, all animals were euthanized and livers explanted. Specimens were embedded in a cryomold with O.C.T. compound (Sakura Finetek, Torrance, CA) and stored at −20°C for a 30-day decay period. Samples were sectioned en face with a slice thickness of 5μm. Consecutive slices (n=7) were stained with hematoxylin and eosin (H&E) for evaluation of tumor necrosis. Normal hepatic parenchyma within the treatment field was stained for Masson's trichrome for type IV collagen to evaluate radiation fibrosis.

### Immunofluorescence

The proliferative index was defined as the percentage of Ki67 positively stained nuclei (100% x Ki67+DAPI+ cells / DAPI+ cells) for 4 high-powered fields per tumor quadrant (x4 quadrants). Microvessel density (MVD) was defined as the number of CD31 positive vessels divided by the total area of liver tissue (vessels/$mm^2$) within each field. Fields were obtained from areas of maximal staining within each tumor quadrant (4 fields per quadrant) for comparisons similar to Gasparini's method as applied by Poon at al. in the setting of HCC (14,15). Tissue slides were digitized at 200× optical magnification with TissueGnostics' TissueFAXS system (TissueGnostics, Los Angeles, CA). Quantitative image analyses of digitized slides for Ki67 and CD31 staining were performed with ImageJ software (version 1.37, National Institutes of Health, Bethesda, MD).

### Statistical Analyses

All data were analyzed with the statistical package STATA (StataCorp, College Station, Texas). Data are reported as means ± standard deviation (SD) or medians with 95% confidence intervals (CI). Comparisons for reported means by t test and for medians by Mann-Whitney test. The Pearson correlation coefficient was used to evaluate the relationship between tumor R2* at baseline and % increase in tumor volume at 2 weeks (16). Rabbits grew a variable number of tumors. A clustering analysis was performed for tumor measurements to examine the impact of clustering by rabbit on standard errors and interpretation of ordinary least squares regression for each comparison. All analyses were two-tailed and considered statistically significant at *P* values less than 0.05.

## RESULTS

### VX2 Tumor Growth

Tumor growth was confirmed in all rabbits. The Y90 group (n=6 rabbits) provided 12 tumors and the control group (n=3 rabbits) provided 6 tumors (2 untreated control rabbits did not reach the 2 week imaging endpoint). At baseline, median tumor volume within the control group and radioembolization group were similar 649.1 versus 531.6mm$^3$,

respectively (p=1.000). The time from implantation to baseline imaging was also similar between the groups at 17.7 versus 16.7 days, respectively (p=0.4512). Therefore, tumors were imaged at similar time and reached similar volume prior to treatment ($^{90}$Y) or no treatment (controls).

### Radioembolization and $^{90}$Y Dosimetry

Mean fluoroscopy time (± SD) was 5.22±2.42 min. A representative DSA is shown in Figure 2 demonstrating antegrade flow to the liver and dense staining of the tumor periphery ("tumor blush"). Technically successful radioembolization was accomplished in 100% (6/6) of cases one day after baseline imaging. All rabbits survived the procedure. The mean calibrated vial activity was 0.96±0.02GBq. Median administered activity was 83.2MBq (CI: 73.3–92.0). Residual vial activity was 11.3% (CI: 7.2–16.8). The median administered dose was 50.4Gy (CI: 44.8–55.9). The lung shunt fraction (LSF) was estimated with hand-held survey meter with a mean LSF of 2.9±1.7%.

### Laboratory Toxicity

Laboratory trends over time are shown in Supplemental Figure 1. Early mild transaminitis after radioembolization was common (observed in 6/6 rabbits) with a 316.7% increase above baseline in ALT at 72 hours and 626.2% increase for AST at 24 hours for Y90 rabbits. These elevations were transient, with ALT values returning to baseline in 4/6 at one week and 6/6 by two weeks. Normal albumin and bilirubin suggested preserved hepatic function for the two-week study. Marked elevation in CK was attributed to the surgical cutdown procedure for femoral arterial access.

### Tumor Volumes and CE-MRI

Represented imaging of VX2 tumors at baseline and after 2 weeks shown in Figure 3. Rabbits treated with $^{90}$Y had significantly reduced median tumor volumes at 2-weeks. These values were 5,769.8 versus 643.7mm$^3$ for control versus Y90 rabbits, respectively (p=0.0246). The median relative increase in tumor sizes beyond baseline was +878.3% versus +160.9% in these groups respectively (p=0.0087). Mean baseline tumor enhancement was similar at 76.8% in controls versus 80.2% in Y90 rabbits (p=0.1685). The percentage of enhancing tissue decreased significantly in the control group to 52.4% versus 71.2% for the $^{90}$Y treated group (p=0.0266).

### BOLD MRI

At baseline, mean R2* values were 78.95±18.02sec$^{-1}$ during room air breathing versus 59.12±12.52sec$^{-1}$ during O2 breathing for Y90 rabbits ( R2*=19.84±19.16sec$^{-1}$). These values (shown in Figure 4) were similar for control rabbits: 71.41±7.57sec$^{-1}$ on room air (p=0.2611) versus 63.81±8.85sec$^{-1}$ on O2 (p=0.3490;  R2*=7.60±4.69sec$^{-1}$).  R2* was similar for control and Y90 groups at baseline (p=0.1113). After radioembolization, one-week imaging showed a reduction in R2* to 59.78±16.64sec$^{-1}$ on room air versus 53.07±13.34sec$^{-1}$ on O$_2$ ( R2*=6.71±7.75sec$^{-1}$). At two weeks, mean R2* values were 65.47±23.05sec$^{-1}$ during room air breathing versus 60.99±21.47sec$^{-1}$ during O$_2$ breathing for Y90 rabbits ( R2*=4.48±9.00sec$^{-1}$). While the  R2* decreased in Y90 tumors, it

increased for control tumors: 74.92±12.74sec$^{-1}$ on room air versus 62.55±19.58sec$^{-1}$ on $O_2$ ( R2*=12.37±12.36sec$^{-1}$). The Pearson correlation coefficient for R2* at baseline and percent increase in tumor size by two weeks was 0.798 for Y90 rabbits (p=0.002) and −0.226 for untreated controls (p=0.667).

### Explant Findings & Histopathology

Representative H&E images are shown in Figure 5. Despite differences in CE-MRI at two weeks, there was no difference in mean pathological necrosis with 46.1% versus 47.1% necrosis in controls and Y90 tumors, respectively (p=0.9287). Trichrome staining of the normal hepatic parenchyma at two weeks was similar in appearance for control and Y90 rabbits without fibrosis.

### Immunofluorescence

Microvessel density (CD31). Positive staining for microvessels was observed within the tumor periphery with no difference in mean MVD detected: 826.8 versus 740.5 vessels/mm$^2$ in control versus Y90 tumors, respectively (p=0.6682). Representative immunostained images are shown in Figure 6.

Proliferative index (Ki67). Ki67 nuclear staining was observed throughout the tumor with the highest density in the viable tumor rim. The mean proliferative index was reduced in Y90 tumors at 30.5% versus 47.5% for controls (p=0.0071).

## DISCUSSION

The evaluation of hepatic VX2 tumors included anatomical imaging, gas-challenge BOLD MRI, and contrast-enhanced MRI in an imaging protocol requiring <1hour. Diminishing R2* after radioembolization was observed over time due to decreased R2* during room air breathing that suggests decreased tumor hypoxia in this animal model (17,18). In controls, increased R2* between baseline and 2-week imaging accompanying increased tumor size suggests increased tumor hypoxia. Moreover, we learned that there was variability in baseline tumor R2* and higher R2* at baseline was correlated with increased tumor growth after radioembolization, indicating decreased treatment efficacy in more hypoxic tumors. Immunofluorescence demonstrated no difference in microvessel density at two weeks between Y90 and control groups, further suggesting the observed differences in R2* were not attributable to decreased perfusion but rather other factors such as decreased tumor metabolism with a decreased proliferative index supporting this mechanism. These findings support the hypothesis that the baseline oxygenation status of tumors treated with radioembolization may relate to treatment response and that Y90 treatment may influence tumor oxygenation over time. Understanding these changes may guide treatment and improve knowledge of tumor biology and physiology following radioembolization.

### Imaging hypoxia.

Our findings may extend to primary and secondary hepatic malignancies where necrosis from chronic diffusion-limit hypoxia is a significant finding. Noninvasive imaging of tumor hypoxia has primarily consisted of nuclear imaging techniques with specialized radiolabeled

nitroimidazoles (19–23), nucleoside conjugates (24,25), or Cu(II)-diacetyl-bis($N^4$-methylthiosemicarbazone) ($^{60}$Cu-ATSM) (26) that are preferentially taken up and retained in severely hypoxic cells to allow positron emission tomography (PET) imaging of these regions. Clinically, PET imaging of hypoxia may someday inform patient prognosis and treatment selection on a patient-specific basis (20,22) and guide planned radiation fields and doses (23,26). However, its use is currently limited since these techniques require an onsite cyclotron, expose patients to ionizing radiation, and are difficult to adopt in the thorax and upper abdomen where motion artifacts can severely influence CT images (27). Alternatively, we implemented broadly applicable MR imaging techniques for rapid noninvasive hypoxia imaging in the liver that have been recently applied after conventional chemoembolization procedures for HCC (28). We propose assessment of tumor hypoxia prior to Y90 may be clinically useful as baseline tumor R2* was correlated with VX2 tumor growth after Y90.

### BOLD imaging.

Previous work has demonstrated that BOLD MRI in the liver allows visualization of R2* changes that accompany gas-challenges, with measurements influenced by a hepatic tissue properties including fibrosis, tumor size, and tumor microvessel density (9,11,12). Imaging of oxygenation with BOLD MRI has been most widely utilized with fMRI in the brain (29) but has also been studied in the kidney (30,31), in tumor models and mixed tumor sites (head and neck, rectum, bladder) (32,33), and also in the liver to evaluate fibrosis (12) and hepatic tumors (11). Signal changes in BOLD MRI of solid tumors have been demonstrated with carbogen gas breathing in humans (33) and these changes could be further explored in relation to radiotherapy efficacy or oxygen electrode measurements in hepatic tumors. Our protocol did not require carbogen gas and allowed rapid assessments of tumor R2* in addition to anatomic and CE-MRI.

### Modulating tumor oxygenation as a future therapeutic strategy.

The absence of $O_2$ attenuates DNA damage, reducing radiotherapeutic efficacy. Moreover, hypoxia also controls gene regulation, influencing tumor behavior: pH, glucose metabolism, growth factors, and Hif-1α stabilization that mediates angiogenesis (VEGF), glycolysis (GLUT1), apoptosis (BNIP), and cell proliferation (IGF2)(34). Strategies to overcome tumor hypoxia (Table 2) include: increasing $O_2$ delivery to tumors, delivering agents that preferentially sensitize hypoxic cells to radiotherapy (nitroimidazoles), and using agents that are preferentially cytotoxic to radioresistant hypoxic tumor cells (anaerobic bacteria (35), Mitomycin C). Understanding tumor oxygenation changes after radioembolization may assist in guiding management for future combination with systemic chemotherapies. Moreover, the increase in R2* observed during room air breathing at baseline suggests that ventilated gases can impact tumor oxygenation status. Therefore, BOLD imaging could be implemented to discern whether tumors are responsive to oxygen breathing and identify ideal patients for home oxygen therapy to increase the oxygenation of hepatic tumors following radioembolization. The safety and tolerability of such approaches should be areas of focus for phase 1 trials; it is anticipated that imaging-guided strategies to evaluate and optimize tumor oxygenation would identify those candidates most likely to benefit from such interventions. Specifically, data for radiotherapy demonstrate tumor hypoxia <10mmHg in head and neck cancer (36), carcinoma of the cervix (17,34), and soft-tissue sarcomas

(19,37) as well as anemia prior to or during radiotherapy (24) confer greatly diminished response, survival, and freedom from local and distant recurrences. We propose MR imaging to monitor tumor oxygenation and guide therapeutic strategies to optimize this parameter for enhanced radiotherapy, a strategy that has been successfully utilized in head and neck cancers and brain metastasis but has not been utilized in radioembolization.

**Limitations.**

The rabbit VX2 model was chosen because the tumor blood supply is almost entirely derived from the hepatic artery, similar to human HCC; in addition, rabbit anatomy is sufficiently large to facilitate catheterization procedures that closely parallel the clinical paradigm (38). This model allows development and validation of new technologies and proofof-concept studies, but is not an appropriate surrogate for therapeutic response to therapy for human HCC, and clinical studies are needed. We also used a fixed, Y90 dose, and future studies should examine dose-dependence of oxygenation changes. A simple oxygen-breathing technique for BOLD MRI was described; however, BOLD signal is influenced by partial volume effects of large blood vessels, motion (respiratory, cardiac pulsation), diffusion, and $B_O$ field inhomogeneities. While large vessels were specifically avoided while drawing ROI and free-breathing gated-sequences were used, more rigorous quantitative BOLD techniques (qBOLD) could be necessary to account for these remaining factors (39). Future work implementing $^{90}Y$ PET/CT imaging techniques to visualize microsphere distributions in relation to hypoxic regions could advance our understanding of these relationships. Finally, despite differences in CE-MRI, there was similar tumor necrosis on pathology at the 2-week time-point for both groups. VX2 tumors are necrotic even in the absence of therapy and Y90 requires more than 2 weeks to generate tumor response by necrosis (median 1.7 months) and size criteria (median 7.6 months) (40). Thus, variability in tumor necrosis and our 2-week endpoint could explain why no difference in pathologic necrosis was observed. Moreover, radiologic-pathologic correlation after liver-directed therapy for HCC is limited and may show complete pathologic necrosis in 14–21% after progressive disease on imaging or viable disease in 32–55% after imaging response (41). Our enhancement evaluations were limited as some lesions were T1 hyper-intense (relative to liver) at baseline and true multiphasic contrast-enhanced imaging could improve these measurements.

## CONCLUSIONS

Intrahepatic VX2 tumors were treated with radioembolization at 50 Gy dosing. In comparison to untreated controls, this resulted in decreased R2* one-week post-treatment that persisted to two weeks. The decrease in this parameter was attributed to decreased hypoxia rather than decreased perfusion because Y90 rabbits had decreased tumor proliferation without diminished microvessel density compared to controls. Moreover, increasing baseline R2* was correlated with increased tumor growth after Y90, indicating decreased treatment efficacy in more hypoxic tumors. This finding may predict radioembolization outcomes. Since all the implemented elements of this study are separately used in clinical practice, phase 1 investigations to bring these together for assessment of tumor oxygenation after radioembolization seem both possible and worthwhile.

## Supplementary Material

Refer to Web version on PubMed Central for supplementary material.

## REFERENCES

1. Chung YE, Kim M-J, Park YN, et al. Varying appearances of cholangiocarcinoma: radiologic-pathologic correlation. Radiographics. 2009;29:683–700. [PubMed: 19448110]

2. Lim JH. Cholangiocarcinoma: morphologic classification according to growth pattern and imaging findings. AJR Am J Roentgenol. 2003;181:819–827. [PubMed: 12933488]

3. Vilgrain V, Paradis V, Menu Y, Mortele KJ. Primary Hepatic Malignant Neoplasms: Radiologic-Pathologic Correlations. … -Pathologic Correlations …. 2005.

4. Powers C, Ros PR, Stoupis C, Johnson WK, Segel KH. Primary liver neoplasms: MR imaging with pathologic correlation. …. 1994.

5. Buetow PC, Buck JL, Ros PR, Goodman ZD. Malignant vascular tumors of the liver: radiologic-pathologic correlation. Radiographics. 1994.

6. Sica GT, Ji H, Ros PR. CT and MR imaging of hepatic metastases. AJR Am J Roentgenol. 2000;174:691–698. [PubMed: 10701611]

7. Chung YE, Park M-S, Park YN, et al. Hepatocellular carcinoma variants: radiologic-pathologic correlation. AJR Am J Roentgenol. 2009;193:W7–W13. [PubMed: 19542386]

8. Brancatelli G, Federle MP, Grazioli L, Carr BI. Hepatocellular carcinoma in noncirrhotic liver: CT, clinical, and pathologic findings in 39 U.S. residents. Radiology. 2002;222:89–94. [PubMed: 11756710]

9. Bristow RG, Hill RP. Hypoxia and metabolism. Hypoxia, DNA repair and genetic instability. Nat Rev Cancer. 2008;8:180–192. [PubMed: 18273037]

10. White SB, Chen J, Gordon AC, et al. Percutaneous Ultrasound Guided Implantation of VX2 for Creation of a Rabbit Hepatic Tumor Model. PLoS ONE. 2015;10:e0123888. [PubMed: 25853660]

11. Guo Y, Jin N, Klein R, et al. Gas challenge-blood oxygen level-dependent (GC-BOLD) MRI in the rat Novikoff hepatoma model. Magn Reson Imaging. 2012;30:133–138. [PubMed: 22055749]

12. Jin N, Deng J, Chadashvili T, et al. Carbogen gas-challenge BOLD MR imaging in a rat model of diethylnitrosamine-induced liver fibrosis. Radiology. 2010;254:129–137. [PubMed: 20032147]

13. Salem R, Thurston KG. Radioembolization with 90Yttrium microspheres: a state-of-the-art brachytherapy treatment for primary and secondary liver malignancies. Part 1: Technical and methodologic considerations. J Vasc Interv Radiol. 2006;17:1251–1278. [PubMed: 16923973]

14. Gasparini G, Harris AL. Clinical importance of the determination of tumor angiogenesis in breast carcinoma: much more than a new prognostic tool. J Clin Oncol. 1995;13:765–782. [PubMed: 7533829]

15. Poon RT-P, Ng IO- L, Lau C, et al. Tumor microvessel density as a predictor of recurrence after resection of hepatocellular carcinoma: a prospective study. J Clin Oncol. 2002;20:1775–1785. [PubMed: 11919234]

16. Zou KH, Tuncali K, Silverman SG. Correlation and simple linear regression. Radiology. 2003;227:617–622. [PubMed: 12773666]

17. Höckel M, Schlenger K, Höckel S, Vaupel P. Hypoxic cervical cancers with low apoptotic index are highly aggressive. Cancer Res. 1999;59:4525–4528. [PubMed: 10493500]

18. Virmani S, Rhee TK, Ryu RK, et al. Comparison of hypoxia-inducible factor-1alpha expression before and after transcatheter arterial embolization in rabbit VX2 liver tumors. J Vasc Interv Radiol. 2008;19:1483–1489. [PubMed: 18922400]

19. Nordsmark M, Alsner J, Keller J, et al. Hypoxia in human soft tissue sarcomas: adverse impact on survival and no association with p53 mutations. Brit J Cancer. 2001;84:1070–1075. [PubMed: 11308256]

20. Rasey JS, Koh WJ, Evans ML, et al. Quantifying regional hypoxia in human tumors with positron emission tomography of [18F]fluoromisonidazole: a pretherapy study of 37 patients. Int J Radiat Oncol Biol Phys. 1996;36:417–428. [PubMed: 8892467]

21. Ziemer LS, Evans SM, Kachur AV, et al. Noninvasive imaging of tumor hypoxia in rats using the 2-nitroimidazole 18F-EF5. Eur J Nucl Med Mol Imaging. 2003;30:259–266. [PubMed: 12552344]

22. Rischin D, Hicks RJ, Fisher R, et al. Prognostic significance of [18F]-misonidazole positron emission tomography-detected tumor hypoxia in patients with advanced head and neck cancer randomly assigned to chemoradiation with or without tirapazamine: a substudy of Trans-Tasman Radiation Oncology Group Study 98.02. J Clin Oncol. 2006;24:2098–2104. [PubMed: 16648512]

23. Rajendran JG, Hendrickson KRG, Spence AM, Muzi M, Krohn KA, Mankoff DA. Hypoxia imaging-directed radiation treatment planning. Eur J Nucl Med Mol Imaging. 2006;33 Suppl 1:44–53. [PubMed: 16763816]

24. Harrison LB, Chadha M, Hill RJ, Hu K, Shasha D. Impact of tumor hypoxia and anemia on radiation therapy outcomes. Oncologist. 2002;7:492–508. [PubMed: 12490737]

25. Riedl CC, Brader P, Zanzonico P, et al. Tumor hypoxia imaging in orthotopic liver tumors and peritoneal metastasis: a comparative study featuring dynamic 18F-MISO and 124I-IAZG PET in the same study cohort. Eur J Nucl Med Mol Imaging. 2008;35:39–46. [PubMed: 17786438]

26. Chao KS, Bosch WR, Mutic S, et al. A novel approach to overcome hypoxic tumor resistance: Cu-ATSM-guided intensity-modulated radiation therapy. Int J Radiat Oncol Biol Phys. 2001;49:1171–1182. [PubMed: 11240261]

27. Chen G, Kung JH, Beaudette KP. Artifacts in computed tomography scanning of moving objects. Semin Radiat Oncol. 2004.

28. Zhang LJ, Zhang Z, Xu J, et al. Carbogen gas-challenge blood oxygen level-dependent magnetic resonance imaging in hepatocellular carcinoma: Initial results. Oncol Lett. 2015;10:2009–2014. [PubMed: 26622788]

29. Ogawa S, Lee TM, Kay AR, Tank DW. Brain magnetic resonance imaging with contrast dependent on blood oxygenation. Proc Natl Acad Sci USA. 1990;87:9868–9872. [PubMed: 2124706]

30. Prasad PV, Edelman RR, Epstein FH. Noninvasive evaluation of intrarenal oxygenation with BOLD MRI. Circulation. 1996;94:3271–3275. [PubMed: 8989140]

31. Tumkur SM, Vu AT, Li LP, Pierchala L, Prasad PV. Evaluation of intra-renal oxygenation during water diuresis: a time-resolved study using BOLD MRI. Kidney Int. 2006;70:139–143. [PubMed: 16572109]

32. Baudelet C, Gallez B. How does blood oxygen level-dependent (BOLD) contrast correlate with oxygen partial pressure (pO2) inside tumors? Magn Reson Med. 2002;48:980–986. [PubMed: 12465107]

33. Taylor NJ, Baddeley H, Goodchild KA, et al. BOLD MRI of human tumor oxygenation during carbogen breathing. J Magn Reson Imaging. 2001;14:156–163. [PubMed: 11477674]

34. Semenza GL. Targeting HIF-1 for cancer therapy. Nat Rev Cancer. 2003;3:721–732. [PubMed: 13130303]

35. Zheng L, Zhang Z, Khazaie K, et al. MRI-Monitored Intra-Tumoral Injection of Iron-Oxide Labeled Clostridium novyi-NT Anaerobes in Pancreatic Carcinoma Mouse Model. PLoS ONE. 2014;9:e116204. [PubMed: 25549324]

36. Brizel DM, Scully SP, Harrelson JM, et al. Radiation therapy and hyperthermia improve the oxygenation of human soft tissue sarcomas. Cancer Res. 1996;56:5347–5350. [PubMed: 8968082]

37. Brizel DM, Sibley GS, Prosnitz LR, Scher RL, Dewhirst MW. Tumor hypoxia adversely affects the prognosis of carcinoma of the head and neck. Int J Radiat Oncol Biol Phys. 1997;38:285–289. [PubMed: 9226314]

38. Geschwind JF, Artemov D, Abraham S, et al. Chemoembolization of liver tumor in a rabbit model: assessment of tumor cell death with diffusion-weighted MR imaging and histologic analysis. J Vasc Interv Radiol. 2000;11:1245–1255. [PubMed: 11099235]

39. He X, Yablonskiy DA. Quantitative BOLD: mapping of human cerebral deoxygenated blood volume and oxygen extraction fraction: default state. Magn Reson Med. 2007;57:115–126. [PubMed: 17191227]

40. Salem R, Gordon AC, Mouli S, et al. Y90 Radioembolization Significantly Prolongs Time to Progression Compared With Chemoembolization in Patients With Hepatocellular Carcinoma. Gastroenterology. 2016;151:1155–1163.e2. [PubMed: 27575820]

41. Riaz A, Memon K, Miller FH, et al. Role of the EASL, RECIST, and WHO response guidelines alone or in combination for hepatocellular carcinoma: radiologic-pathologic correlation. J Hepatol. 2011;54:695–704. [PubMed: 21147504]

**Summary Statement:**

MRI measurements tracked changes after radioembolization and correlated with resistance to therapy as measured by increased tumor growth at 2 weeks

**Key Points:**

MRI measurements demonstrate measurable changes after radioembolization during gas-challenge examinations. Pre-procedural MRI metrics may predict therapeutic resistance to radioembolization. Decreased tumor proliferation was observed at 2 weeks follow radioembolization.
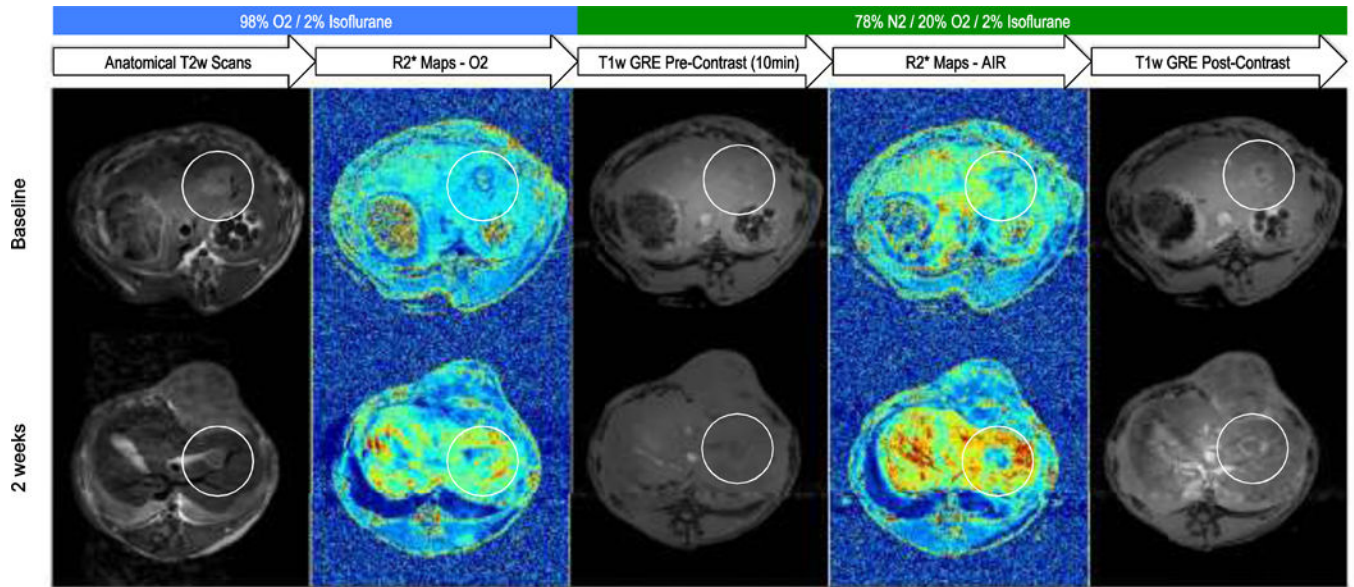
**Figure 1.**

Imaging protocol for evaluation of rabbit VX2 tumors (circled) and representative images at baseline and 2 weeks post yttrium-90 radioembolization. Rabbits were maintained on 98% O2 with 2% isoflurane gas anesthesia at 1L/min. Anatomical T2-weighted imaging was used to identify intrahepatic VX2 tumor growth as 1–2 cm heterogeneously hyperintense lesions. R2* mapping with complete tumor coverage was performed using a 4-echo respiratory-gated GRE sequence during oxygen breathing and gas anesthesia was subsequently switched to room air (20% O2, 78% N2, 2% isoflurane). Pre-contrast T1-weighted GRE imaging was acquired and at least 10 minutes were allowed prior to steady-state R2* mapping during room air breathing. Contrast-enhanced imaging after administration of dimeglumine gadopentate (Magnevist) allowed evaluation of tumor enhancement.
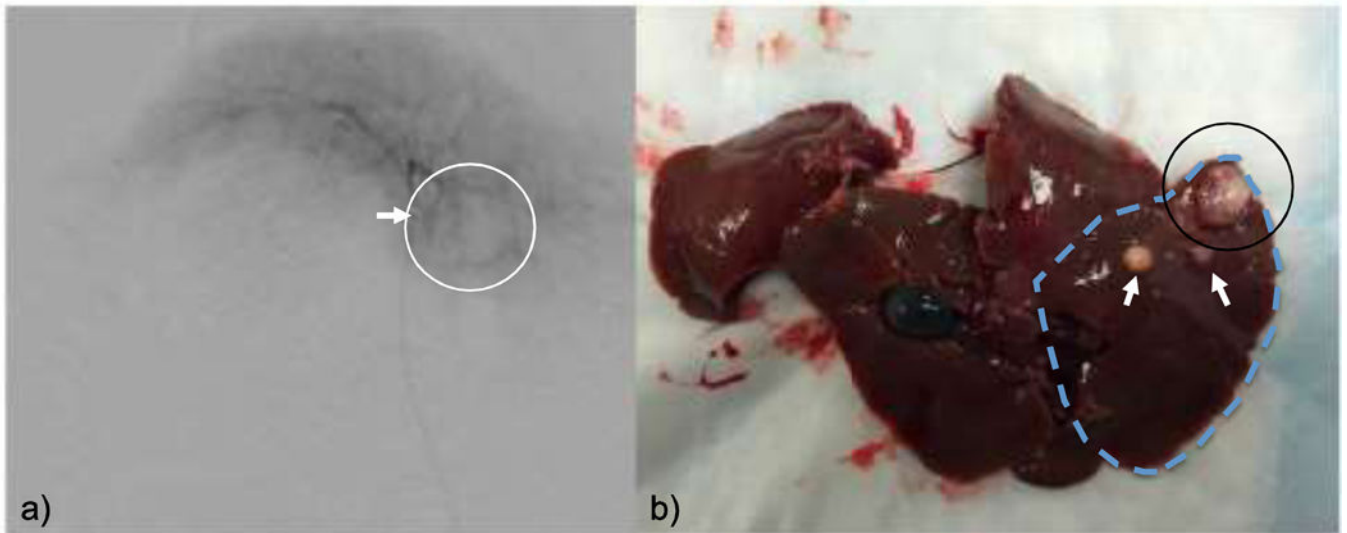
**Figure 2.**
**a)** Digital subtraction angiography after x-ray fluoroscopy guidance of radio-opaque microcatheter tip (arrow) positioning in the proper hepatic artery confirms tumor blush (circle) in the left lateral lobe with dominant supply from the left hepatic artery. **b)** Gross pathologic photograph of tumor (circled) in the left lateral lobe (outlined) with several smaller satellite lesions (arrows). The treated tumor appears small, pale, and retracted from the adjacent parenchyma with puckering in the tumor periphery.
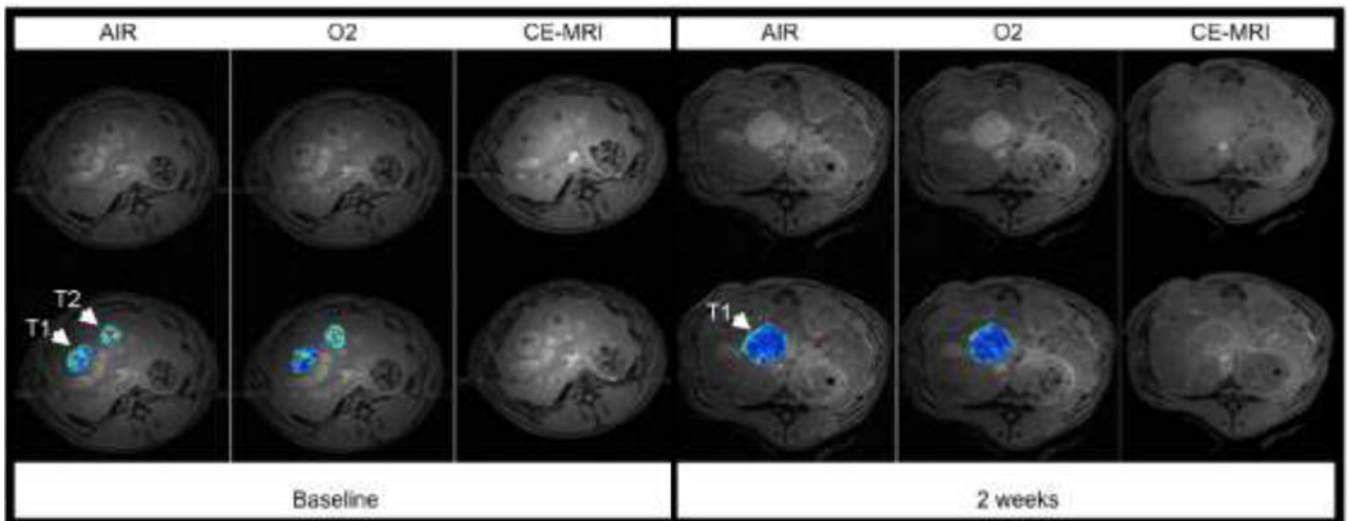
**Figure 3.**
Imaging at baseline (left) and 2-weeks post-radioembolization (right) after infusion of 94MBq $^{90}$Y to the whole liver. At baseline, both lesions enhance on contrast-enhanced (CE) imaging and high R2* values are present within areas of central necrosis in each tumor (1 and 2). After 2 weeks, tumor 1 has enlarged and shows considerable necrosis with peripheral rim enhancement on CE-MRI. Gas challenge resulted in little to no increase in R2* during room air breathing at this time.
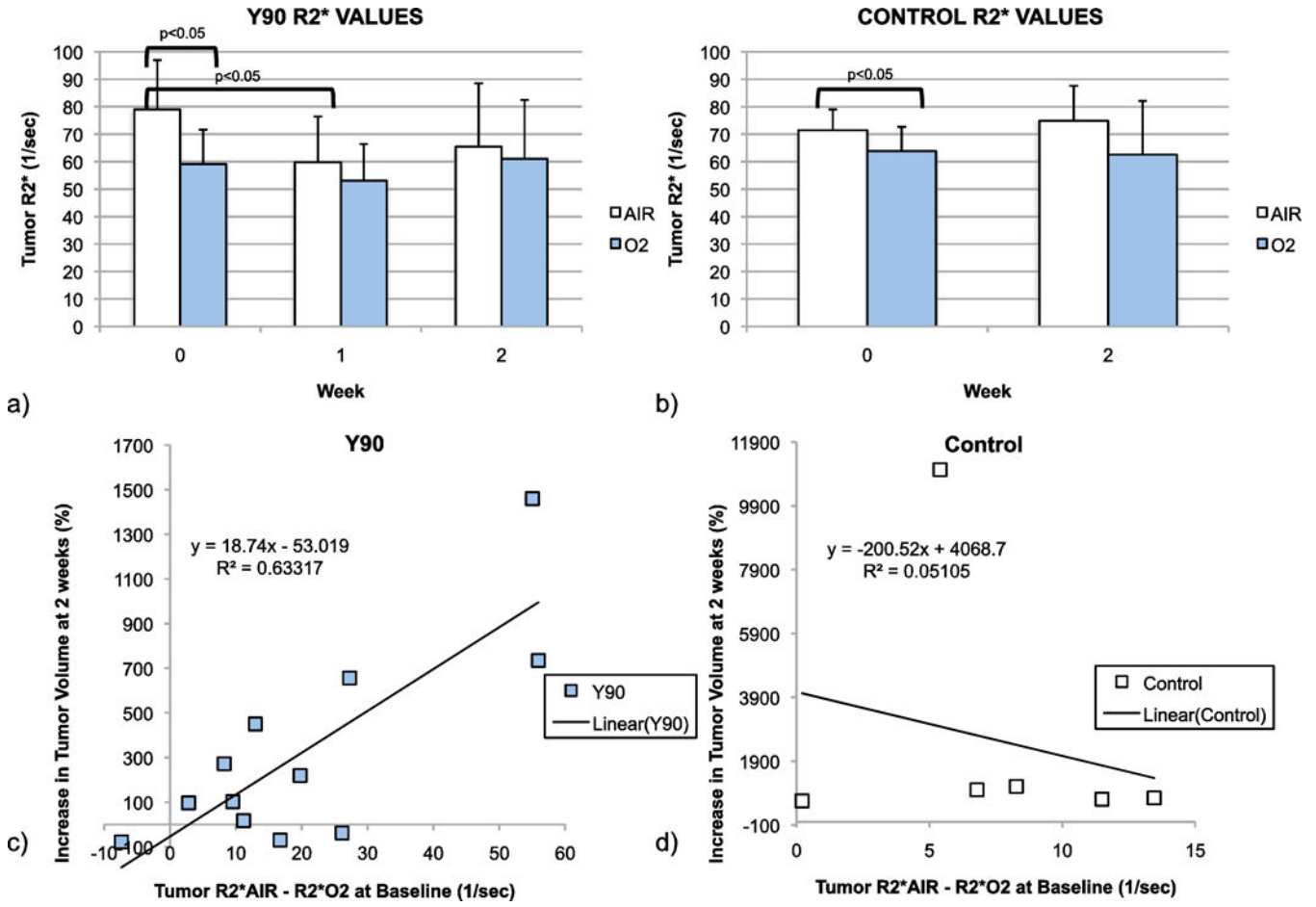
**Figure 4.**
Whole tumor R2* changes during room air (AIR) versus oxygen (O2) breathing. Room air breathing increased R2* values within VX2 tumors at baseline due to increased paramagnetic susceptibility from deoxyHb. a) Over time, rabbits treated with radioembolization (n=12 tumors, 6 rabbits) had reductions in R2* values during room air breathing at 1 and 2 weeks post-radioembolization while b) untreated control rabbits (n=6 tumors, 3/5 rabbits) demonstrated a stable to slightly increased R2* during room air breathing at 2 weeks. c) Tumor growth rate was higher in untreated control rabbits and while the gas-challenge signal was maintained in control rabbits, tumors treated with radioembolization had a drop in this signal suggesting decreased tumor hypoxia.
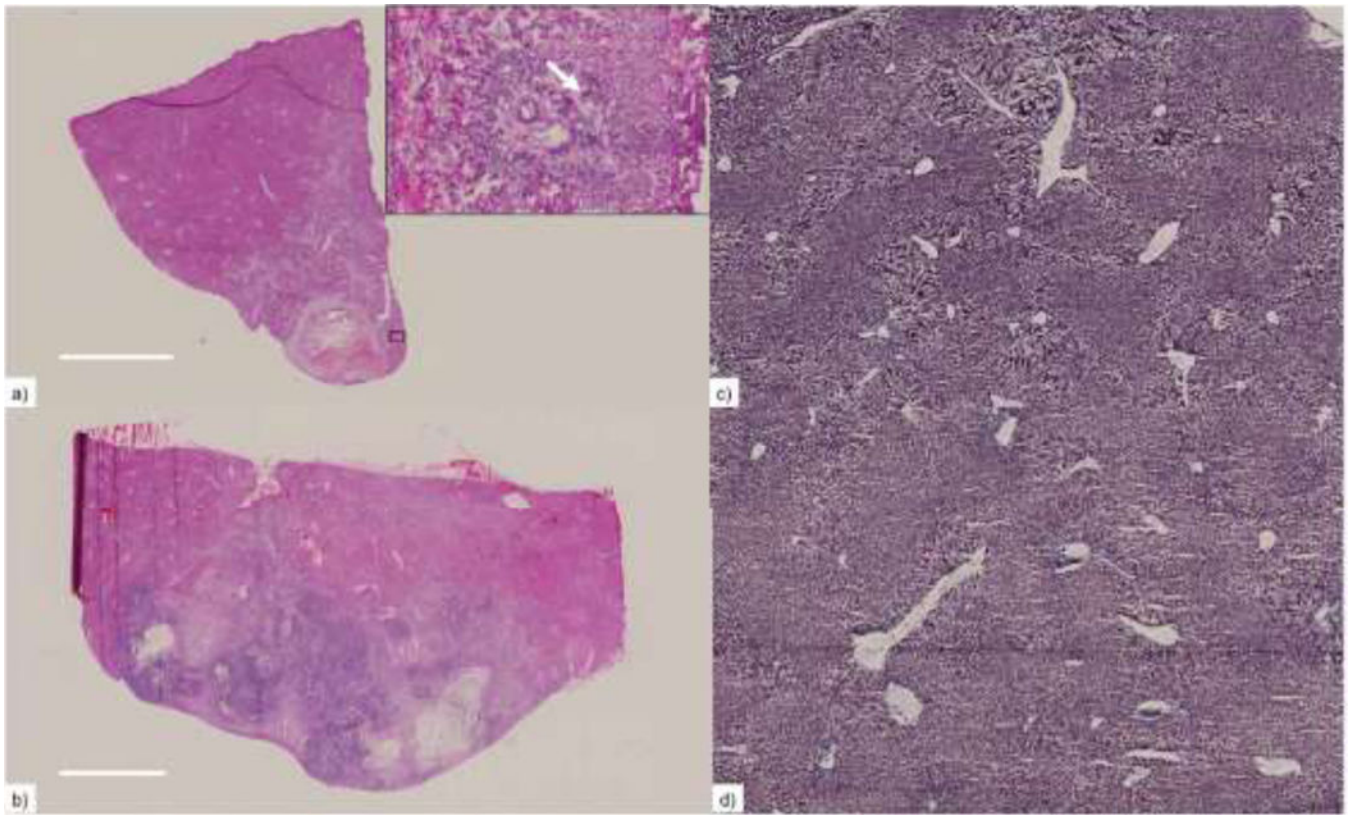
**Figure 5.**
Histopatholgy of VX2 tumors following yttrium-90 radioembolization (a,c) versus untreated control rabbit (b,d). a) H&E demonstrates necrosis with inset at 200x optical magnification demonstrating microsphere (arrow) in the tumor periphery. b) Untreated control tumors demonstrated viable tissue and focal areas of necrosis (scale bar = 5mm). Masson's trichrome staining at 25x optical magnification shows no difference in fibrosis between c) yttrium-90 treated rabbits and d) control rabbits at 2-weeks.
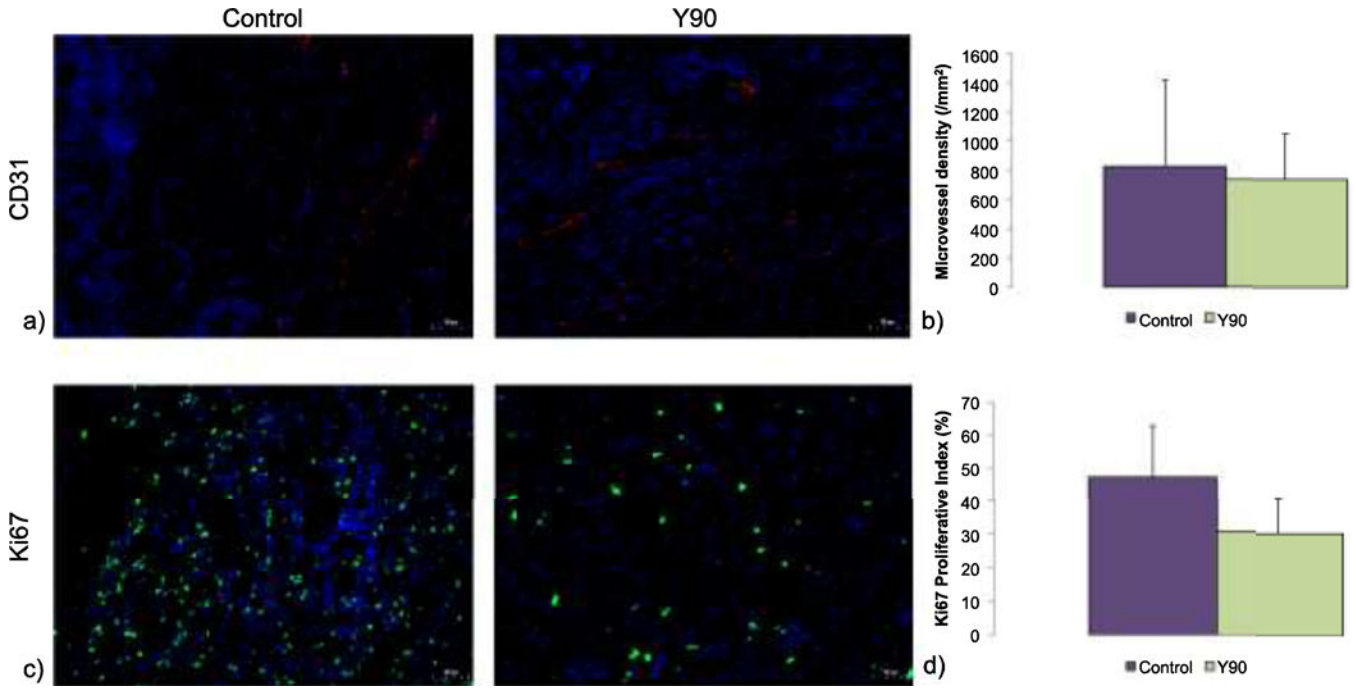
**Figure 6.**
Immunofluorescence staining of VX2 tumors following yttrium-90 radioembolization (right) versus untreated control rabbits (left). a) CD31 positive staining (red) at 200x optical magnification demonstrated similar microvessel density (scale bar = 50μm) within the tumor periphery for the two groups and b) quantification showed no difference in MVD (p=0.6682). c) Increased Ki67 positive nuclear staining (green) was observed in untreated controls that had d) increased proliferative index in comparison to ^{90}Y treated VX2 tumors (p=0.0071).

**Table 1:**

MRI Pulse Sequences

| Purpose | Sequences | Scan Parameters |
|---|---|---|
| Anatomic Imaging | 3D T2-Weighted Turbo Spin Echo (TSE) | TR/TE=1053/30ms, turbo-factor=12, 256×256 matrix, 130×130mm FOV, 30 slices at 1.5mm thickness, 200Hz/px Bandwidth. |
| BOLD R2* Measurements | R2* 3D Gradient recalled echo (GRE) | TR=1730ms, 30° FA, GRE ETL=4, echo-spacing (ES)=3.72ms, 256×256 matrix, 120×120 mm FOV, 1.0mm slice thickness, 500Hz/px Bandwidth. |
| Tumor Enhancement | T1 3D Gradient recalled echo (GRE) | TR/TE=1730/2.42ms, 90° FA, 256×256 matrix, 120×120 mm FOV, 1.5mm slice thickness, 500Hz/px Bandwidth. |

Author Manuscript

Author Manuscript

Author Manuscript

Author Manuscript

**Table 2.**

Radiosensitizing Agents and Oxygenation

| Mechanism | Description | Clinical Use |
|---|---|---|
| **Targeting hypoxic cells** | | |
| Mitomycin C | Causes alkylation and crosslinking of DNA under anaerobic conditions | Hepatocellular carcinoma |
| Tirapazamine | Causes oxidative damage to pyrimidines | Non-small cell lung cancer (brain metastases), head & neck cancers |
| Cisplatin | Crosslinks DNA | Hepatocellular carcinoma |
| **Increasing tumor O2** | | |
| Efaproxiral | Decreases the oxygen binding affinity of hemoglobin through allosteric modification | Non-small cell lung cancer, metastatic breast cancer (brain metastases) |
| Perfluorocarbon O2 carriers | Increases $O_2$ concentrations | Experimental |
| **Sensitization to radiotherapy** | | |
| 5-FU | Inhibits DNA synthesis (thymidine analog) | Metastatic colorectal cancer |
| Irinotecan | Inhibits topoisomerase I | Metastatic colorectal cancer |
| Paclitaxel | Inhibits microtubules | Metastatic breast cancer |
| Gemcitabine | Produces metabolites that cause early termination of DNA strands | Intrahepatic cholangiocarcinoma, metastatic breast cancer, pancreatic cancer |
| Motexafin gadolinium | Sensitizes cancer cells to ionizing radiation through targeting redox-dependent pathways and serves as an MRI contrast agent | Non-small cell lung cancer (brain metastases) |